PHILOSOPHICAL TRANSACTIONS OF THE ROYAL SOCIETY A

Phil. Trans. R. Soc. A (2011) **369**, 2155–2163
doi:10.1098/rsta.2011.0017

Convergence of a three-dimensional quantum lattice Boltzmann scheme towards solutions of the Dirac equation

By Denis Lapitski and Paul J. Dellar*

OCIAM, Mathematical Institute, University of Oxford, 24–29 St Giles', Oxford OX1 3LB, UK

We investigate the convergence properties of a three-dimensional quantum lattice Boltzmann scheme for the Dirac equation. These schemes were constructed as discretizations of the Dirac equation based on operator splitting to separate the streaming along the three coordinate axes, but their output has previously only been compared against solutions of the Schrödinger equation. The Schrödinger equation arises as the non-relativistic limit of the Dirac equation, describing solutions that vary slowly compared with the Compton frequency. We demonstrate first-order convergence towards solutions of the Dirac equation obtained by an independent numerical method based on fast Fourier transforms and matrix exponentiation.

Keywords: quantum lattice Boltzmann; Dirac equation; Schrödinger equation

1. Introduction

The lattice Boltzmann approach to computational hydrodynamics relies on the Navier–Stokes equations describing slowly varying solutions of the Boltzmann equation. The same property holds when the continuous velocity space of the standard kinetic theory is truncated to obtain a discrete Boltzmann equation, which we write as [1–3]

$$(\partial_t + \boldsymbol{\xi}_i \cdot \nabla) f_i = \sum_{j=0}^{n} \Omega_{ij} (f_j - f_j^{(0)}), \tag{1.1}$$

for $i = 0, \ldots, n$. The distribution functions f_i propagate in the directions given by the discrete velocities $\boldsymbol{\xi}_i$, and relax towards their equilibrium values $f_i^{(0)}$ through the action of the collision matrix Ω_{ij}.

The quantum lattice Boltzmann (QLB) schemes introduced by Succi & Benzi [4] exploit the structural similarities between the discrete Boltzmann equation and the Dirac equation of quantum electrodynamics [5]. Both are linear, symmetric, hyperbolic systems with algebraic source terms, so numerical algorithms for the Dirac equation may be obtained by applying the same techniques that lead from the discrete Boltzmann equation to lattice Boltzmann schemes for

*Author for correspondence (dellar@maths.ox.ac.uk).

One contribution of 26 to a Theme Issue 'Discrete simulation of fluid dynamics: methods'.

hydrodynamics (see [2,6,7]). QLB schemes may also be interpreted as cellular automata that evolve probability amplitudes (qbits) rather than bits [8,9]. Palpacelli & Succi [10] have surveyed recent applications of QLB schemes to simulate the Schrödinger equation of non-relativistic quantum mechanics. The Schrödinger equation describes slowly varying solutions of the Dirac equation, in close analogy with the derivation of the Navier–Stokes equations as describing slowly varying solutions of the Boltzmann equation. However, attention has not previously been paid to the properties of QLB schemes for computing solutions to the Dirac equation itself.

2. The Dirac equation

The Dirac equation offers a quantum mechanical description of an electron that is compatible with special relativity [5]. Its standard form is

$$(\partial_t + c\boldsymbol{\alpha}\cdot\nabla)\psi = -\mathrm{i}\omega_c\beta\psi + \mathrm{i}g\psi, \tag{2.1}$$

where c is the light speed, $\hbar$ is the reduced Planck's constant and $\omega_c = mc^2/\hbar$ is the Compton frequency for a particle of mass m. The wave function ψ is a column vector with four components, β is a 4×4 matrix, and $\boldsymbol{\alpha} = (\alpha^x, \alpha^y, \alpha^z)$ is a collection of three 4×4 matrices, so that $\boldsymbol{\alpha}\cdot\nabla = \alpha^x\partial_x + \alpha^y\partial_y + \alpha^z\partial_z$. The last term couples the wave function to an applied scalar potential V via the coefficient $g = qV/\hbar$, where $q>0$ is the modulus of the charge on an electron. This sign convention was used in previous QLB schemes, but it differs from that in Berestetskii *et al.* [5].

The 4×4 matrices α^i and β may be written in block form as

$$\alpha^i = \begin{pmatrix} 0 & \sigma^i \\ \sigma^i & 0 \end{pmatrix} \quad \text{and} \quad \beta = \begin{pmatrix} \mathsf{I} & 0 \\ 0 & -\mathsf{I} \end{pmatrix}, \tag{2.2}$$

where I is the 2×2 identity matrix. The off-diagonal blocks are Pauli spin matrices,

$$\sigma^x = \begin{pmatrix} 0 & 1 \\ 1 & 0 \end{pmatrix}, \quad \sigma^y = \begin{pmatrix} 0 & -\mathrm{i} \\ \mathrm{i} & 0 \end{pmatrix} \quad \text{and} \quad \sigma^z = \begin{pmatrix} 1 & 0 \\ 0 & -1 \end{pmatrix}, \tag{2.3}$$

which satisfy the well-known commutation relations [5]

$$\sigma^i\sigma^j - \sigma^j\sigma^i = 2\mathrm{i}\epsilon_{ijk}\sigma^k, \tag{2.4}$$

where ϵ_{ijk} is the alternating Levi-Civita tensor. The α matrices are all Hermitian, and hence diagonalizable, but the commutators of their non-zero blocks do not vanish. There is thus no basis in which the α matrices are simultaneously diagonal.

Writing the wave function as $\psi = (\phi_1^+, \phi_2^+, \phi_1^-, \phi_2^-)^{\mathsf{T}}$, the $\pm$ superscripts correspond to components with positive and negative energies. For a free particle, these oscillate in proportion to $\exp(\mp\mathrm{i}\omega_c t)$ in the long-wave limit. The subscripts 1 and 2 label the two different spin states. To derive the Schrödinger equation, one writes $\psi = (\Phi_1^+, \Phi_2^+, \Phi_1^-, \Phi_2^-)^{\mathsf{T}}\exp(-\mathrm{i}\omega_c t)$ to transform away the rest energy of the + states, assumes $\partial_t\Phi_{1,2}^- \ll 2\mathrm{i}\omega_c\Phi_{1,2}^-$, equivalent to a non-relativistic limit, and substitutes the resulting adiabatic approximations for $\Phi_{1,2}^-$ into the evolution equations for $\Phi_{1,2}^+$. Palpacelli & Succi [10] give a derivation in this notation.

3. Quantum lattice Boltzmann schemes

The Dirac and discrete Boltzmann equations are both linear, symmetric, hyperbolic systems with algebraic source terms. However, the discrete Boltzmann equation is highly unusual among multi-dimensional hyperbolic systems in possessing one-dimensional characteristic curves of the form $(\mathbf{x}, t) = (\mathbf{x}_0 + s\boldsymbol{\xi}_i, t_0 + s)$, as parametrized by s. All one may expect in general is the existence of three-dimensional characteristic surfaces in four-dimensional $(\mathbf{x}, t)$ space [11].

The three α matrices are not simultaneously diagonalizable, so the characteristics of the Dirac equation are indeed three-dimensional surfaces, the light cones of special relativity. Discontinuities in the initial conditions are confined to propagating along these surfaces, but there are no one-dimensional characteristic curves to integrate along. The approach that leads from the discrete Boltzmann equation to a lattice Boltzmann scheme (as in [12]) thus cannot be employed.

Instead, multi-dimensional QLB schemes use operator splitting to approximate solutions to the three-dimensional Dirac equation using solutions of one-dimensional Dirac equations in which spatial dependences in the other two directions are temporarily neglected. For instance, neglecting dependence on y and z leads to

$$(\partial_t + c\alpha^x \partial_x)\psi = -\tfrac{1}{3}\mathrm{i}\omega_\mathrm{c}\beta\psi + \tfrac{1}{3}\mathrm{i}g\psi. \tag{3.1}$$

The factor of 1/3 on the right-hand side arises from dividing the algebraic terms into three equal parts, one associated with each spatial direction [7]. Each of these one-dimensional Dirac equations does have characteristic curves, since the α matrices are Hermitian and thus diagonalizable. Equation (3.1) and its analogues in y and z may thus be evolved forward in time using the one-dimensional QLB algorithm described by Succi & Benzi [4] and Succi [6]. It is convenient to choose units in which $c = 1$ and $\hbar = 1$, so $\Delta x = \Delta t$ and $\omega_\mathrm{c} = m$.

Existing QLB schemes begin with the Majorana form of the Dirac equation [5], but the same approach may be applied to the standard form (2.1) in which the algebraic terms are diagonal. The only disadvantage is that α^y must be diagonalized by a complex matrix. The two approaches based on the Majorana and standard forms agree to within numerical round-off errors.

The three α matrices in the standard form (2.1) may be diagonalized as

$$X^\dagger \alpha^x X = Y^\dagger \alpha^y Y = Z^\dagger \alpha^z Z = \beta, \tag{3.2}$$

where † denotes the Hermitian transpose, by the three unitary matrices

$$X = \frac{1}{\sqrt{2}}\begin{pmatrix} 1 & 0 & -1 & 0 \\ 0 & 1 & 0 & -1 \\ 0 & 1 & 0 & 1 \\ 1 & 0 & 1 & 0 \end{pmatrix}, \quad Y = \frac{1}{\sqrt{2}}\begin{pmatrix} 0 & \mathrm{i} & 0 & 1 \\ -\mathrm{i} & 0 & \mathrm{i} & 0 \\ -1 & 0 & -1 & 0 \\ 0 & -1 & 0 & -\mathrm{i} \end{pmatrix}$$

and

$$Z = \frac{1}{\sqrt{2}}\begin{pmatrix} 1 & 0 & 0 & -1 \\ 0 & -1 & 1 & 0 \\ 1 & 0 & 0 & 1 \\ 0 & 1 & 1 & 0 \end{pmatrix}. \tag{3.3}$$

Thus, the streaming step in x consists of multiplying ψ by $X^\dagger$, streaming $\hat{\psi} = X^\dagger \psi$ in the x-directions by $\pm\Delta x$, and finally multiplying $\hat{\psi}$ by X to undo the transformation. The first QLB schemes suffered from numerical artefacts owing to applying the X and $X^\dagger$ matrices in the wrong order [13]. We also use operator splitting to separate the spatial derivatives from the algebraic terms, which are diagonal in the standard representation. The + components are

$$\partial_t \phi^+_{1,2} = \tfrac{1}{3}\mathrm{i}(g-m)\phi^+_{1,2}, \tag{3.4}$$

which we discretize using the Crank–Nicolson scheme to obtain

$$\frac{\phi^+_{1,2}(t+\Delta t) - \phi^+_{1,2}(t)}{\Delta t} = \frac{1}{6}\mathrm{i}(g-m)(\phi^+_{1,2}(t+\Delta t) + \phi^+_{1,2}(t)). \tag{3.5}$$

The solution, and its analogue for $\phi^-_{1,2}(t+\Delta t)$, may be expressed in the manifestly unitary form

$$\phi^\pm_{1,2}(t+\Delta t) = \phi^\pm_{1,2}(t)\frac{1 + \mathrm{i}\Delta t(g \mp m)/6}{1 - \mathrm{i}\Delta t(g \mp m)/6}. \tag{3.6}$$

Writing the transformed post-collisional wave function as $\hat{\psi} = (\hat{\phi}^+_1, \hat{\phi}^+_2, \hat{\phi}^-_1, \hat{\phi}^-_2)^\mathsf{T}$, the QLB step for colliding and streaming in x may be written as

$$\psi(x, t+\Delta t) = X \begin{pmatrix} \hat{\phi}^+_{1,2}(x-\Delta t, t) \\ \hat{\phi}^-_{1,2}(x+\Delta t, t) \end{pmatrix}, \quad \text{where } \hat{\psi}(x,t) = X^\dagger \begin{pmatrix} \phi^+_{1,2}(x, t+\Delta t) \\ \phi^-_{1,2}(x, t+\Delta t) \end{pmatrix}. \tag{3.7}$$

The full QLB scheme combines this step with analogous collision and streaming steps in the y- and z-directions, as diagonalized by the Y and Z matrices.

4. Free particle

We apply the QLB scheme described above to initial conditions in which the positive energy, spin-up component ϕ^+_1 is a spherically symmetric Gaussian wavepacket with spread Δ_0, as in Palpacelli & Succi [7],

$$\phi^+_1(x,y,z,t) = (2\pi\Delta_0^2)^{-3/4} \exp\left(-\frac{x^2+y^2+z^2}{4\Delta_0^2}\right). \tag{4.1}$$

The other three components ϕ^+_2 and $\phi^-_{1,2}$ are initially set to zero. We study the dispersion of the wavepacket over time, as measured by the spread Δ defined by

$$\Delta = \frac{(\int (1/3)|\mathbf{x}|^2 |\phi^+_1|^2 \,\mathrm{d}\, V)^{1/2}}{(\int |\phi^+_1|^2 \,\mathrm{d}\, V)^{1/2}}. \tag{4.2}$$

We approximate these integrals using the trapezium rule, which is exponentially accurate for equally spaced points in a domain with periodic boundary conditions.

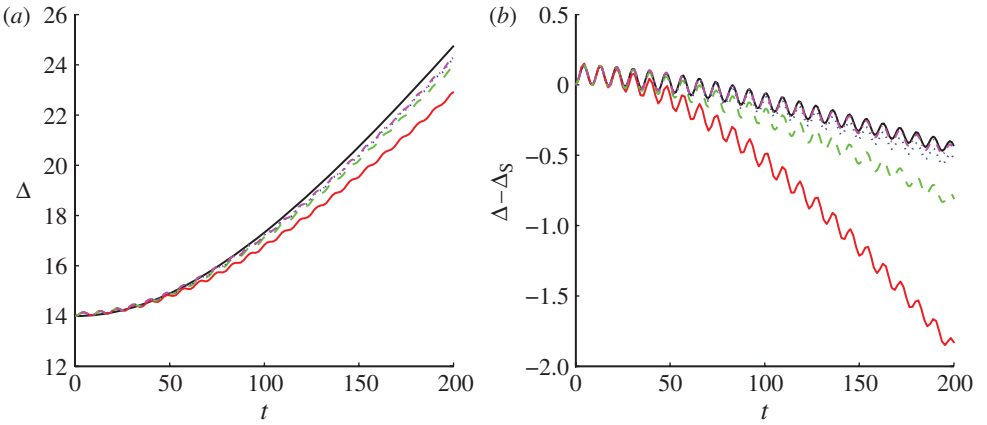

Figure 1. (*a*) Evolution of the spread Δ for different numbers of grid points N. (*b*) Difference between the computed Δ and the Schrödinger solution Δ_S. Lower solid line, $N=128$; dashed line, $N=256$; dotted line, $N=512$; dashed–dotted line, $N=1024$; upper solid line, (*a*) Schrödinger exact solution and (*b*) Dirac exact solution. (Online version in colour.)

According to the Schrödinger equation, the spread of this wavepacket grows as

$$\Delta_S(t) = \left(\Delta_0^2 + \frac{\hbar^2 t^2}{4m^2\Delta_0^2}\right)^{1/2}. \tag{4.3}$$

Figure 1*a* shows the measured spread for a free particle with $m=0.35$ and $\Delta_0=14$ in a cube with side length $\ell=200$ and periodic boundary conditions. All these quantities are expressed in natural units with $c=1$ and $\hbar=1$. The cube was discretized using N^3 points for $N=128$, 256, 512, 1024. The computed spreads on the different grids all follow the general trend of the Schrödinger solution Δ_S, but they are all subject to superimposed high-frequency oscillations. Similar oscillations were seen in one-dimensional computations by Valdivieso & Muñoz [14].

Figure 1*b* shows the differences between the measured spreads and the spread Δ_S predicted by the Schrödinger equation. Also shown is the spread Δ_D for a highly accurate numerical solution to the Dirac equation, computed as described in §4*a*. High-frequency oscillations are also present in Δ_D. These oscillations, at frequencies comparable to the Compton frequency, are an intrinsic feature of the Dirac equation as a relativistic theory that accounts for a particle's rest energy mc^2 as well as kinetic energy owing to its motion. Figure 2*a* shows the second-order convergence of the measured spreads towards the spread Δ_D of the reference solution. Further confirmation is given in figure 2*b*, showing the first-order convergence of the four fields $\phi^{\pm}_{1,2}$ towards the reference solution in the L_2 norm.

(*a*) *Reference solutions*

In the absence of a potential ($g=0$), the Dirac equation becomes a linear partial differential equation with constant coefficients. It is thus amenable to Fourier transform techniques. Substituting $\psi(\mathbf{x},t)=\tilde{\psi}(t)\exp(\mathrm{i}\mathbf{k}\cdot\mathbf{x})$ into

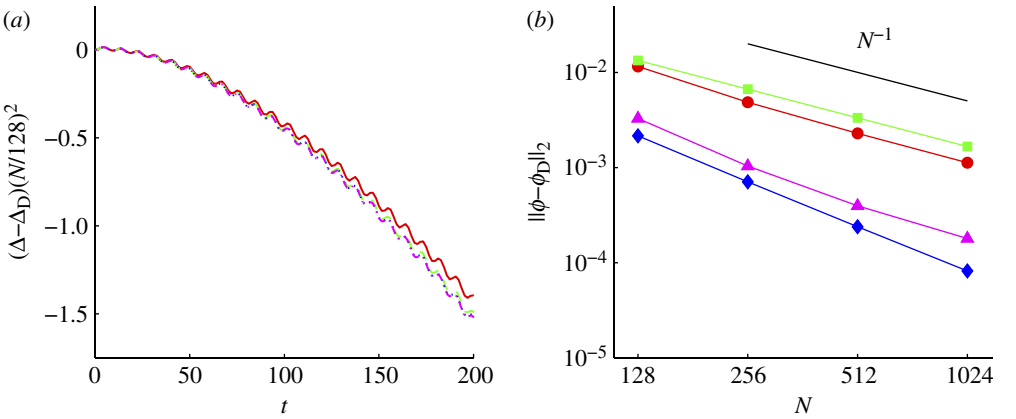

Figure 2. (*a*) Second-order convergence of the spreads Δ towards the reference solution Δ_D of the Dirac equation. (*b*) First-order convergence of the moduli of the four fields $\phi^{\pm}_{1,2}$ towards the reference solution $\phi^{\pm}_{1,2\,D}$ at $t=200$. (*a*) Solid line, $N=128$; dashed line, $N=256$; dotted line, $N=512$; dashed–dotted line, $N=1024$. (*b*) Filled circles, ϕ_1^+; filled squares, ϕ_2^+; filled diamonds, ϕ_1^-; filled triangles, ϕ_2^-. (Online version in colour.)

equation (2.1) leads to

$$\mathrm{i}\partial_t\tilde{\psi} = \mathsf{H}_{\mathbf{k}}\tilde{\psi}, \tag{4.4}$$

with the 4×4 matrix Hamiltonian $\mathsf{H}_{\mathbf{k}} = m\beta + \boldsymbol{\alpha}\cdot\mathbf{k}$. The solution to equation (4.4) is given by $\tilde{\psi}(t) = \exp(-\mathrm{i}t\mathsf{H}_{\mathbf{k}})\tilde{\psi}(0)$, where

$$\exp(-\mathrm{i}t\mathsf{H}_{\mathbf{k}}) = \cos(\Omega t)\mathsf{I} - \left(\frac{\mathrm{i}}{\Omega}\right)\sin(\Omega t)\mathsf{H}_{\mathbf{k}}, \tag{4.5}$$

and $\Omega = (m^2 + |\mathbf{k}|^2)^{1/2}$. Exponentially accurate numerical solutions in periodic domains may be computed by expressing the initial ψ as a Fourier series, and evolving each Fourier coefficient using equation (4.5). Transformations between grid-point values and Fourier coefficients may be computed efficiently using fast Fourier transforms.

5. Particle in a harmonic potential

We consider the same initial conditions, with zero initial momentum, confined by a harmonic potential $V(\mathbf{x}) = -(1/2)m\omega_0^2|\mathbf{x}|^2$ under our sign convention. Setting $\omega_0 = 1/(2m\Delta_0^2)$ leads to the initial spread Δ_0 of the wavepacket being preserved by subsequent evolution under the Schrödinger equation. For this test case, we consider a cube with side length $\ell = 200$, mass $m = 0.1$ and initial spread $\Delta_0 = 14$. To avoid the convergence properties being affected by discontinuities in the gradient of V at periodic boundaries, we approximate $|\mathbf{x}|^2$ by $v(x) + v(y) + v(z)$, where the function $v(x)$ is the first six terms of a Fourier cosine series approximation to x^2 in $[-\ell, \ell]$.

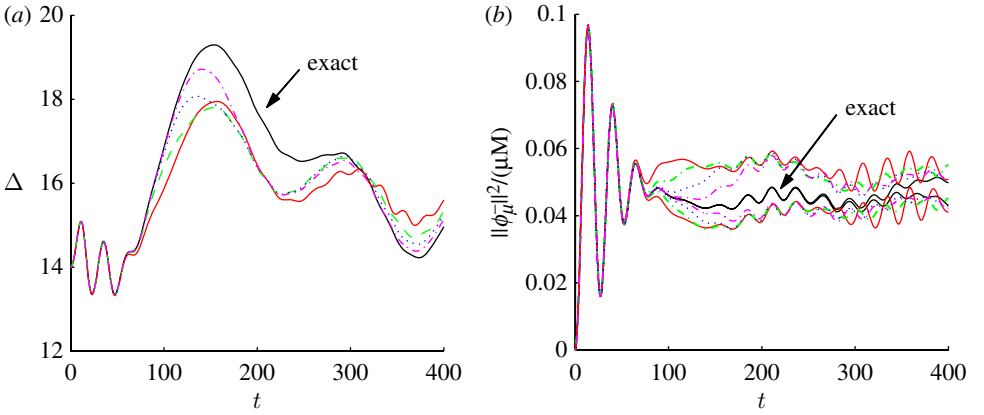

Figure 3. Evolution of (*a*) the spread Δ and (*b*) the relative magnitudes $||\phi_\mu^-||/(\mu M)$ of the negative-energy components, for different grid resolutions N. Solid line, $N=128$; dashed line, $N=256$; dotted line, $N=512$; dashed–dotted line, $N=1024$; solid line marked by arrow, exact solution. (Online version in colour.)

(*a*) *Reference solutions*

A spatially varying potential couples the different Fourier modes, so exact solutions cannot be computed as Fourier series. However, accurate approximations may be obtained by splitting the Hamiltonian. The free-particle Hamiltonian $\mathsf{H}_\mathbf{k}$ decouples into one 4×4 block for each Fourier mode, as above. The coupling Hamiltonian $\mathsf{H}_g=-g(\mathbf{x})\mathsf{I}$ is diagonal in physical space, with a time-evolution operator given by

$$[\exp(-\mathrm{i}\Delta t\mathsf{H}_g)\psi](\mathbf{x},t)=\exp(\mathrm{i}\Delta t g(\mathbf{x}))\psi(\mathbf{x},t). \tag{5.1}$$

Thus, g is *minus* the dimensionless potential energy in our sign convention. Strang splitting approximates the coupled evolution to second-order accuracy by using

$$\exp(-\mathrm{i}\Delta t\mathsf{H})=\exp(-\tfrac{1}{2}\mathrm{i}\Delta t\mathsf{H}_g)\exp(-\mathrm{i}\Delta t\mathsf{H}_\mathbf{k})\exp(-\tfrac{1}{2}\mathrm{i}\Delta t\mathsf{H}_g)+\mathcal{O}(\Delta t^3). \tag{5.2}$$

For the reference computations, we used Forest & Ruth's [15] fourth-order accurate splitting into seven steps, with an overall time step $\Delta t=1.0$ and 128^3 Fourier modes. This solution was indistinguishable, for comparison purposes, from one computed with $\Delta t=0.25$ and 256^3 Fourier modes.

(*b*) *Results*

Figure 3*a* shows the evolution of the spread Δ for the reference solution, and for four QLB solutions on N^3 grids with $N=128$, 256, 512, 1024. All solutions are in good agreement for $0\le t\lesssim 75$, after which the initially regular oscillations are disrupted by negative-energy states reflecting from the periodic boundaries. The solutions appear very sensitive to small errors owing to the finite resolution, as shown by the diverging trajectories. Figure 3*b* shows similar behaviour in the squared L_2 norms of the negative-energy components $\phi_{1,2}^-$, as normalized by $M=\sum||\phi_{1,2}^\pm||^2$ and $2M$, respectively. These two components are

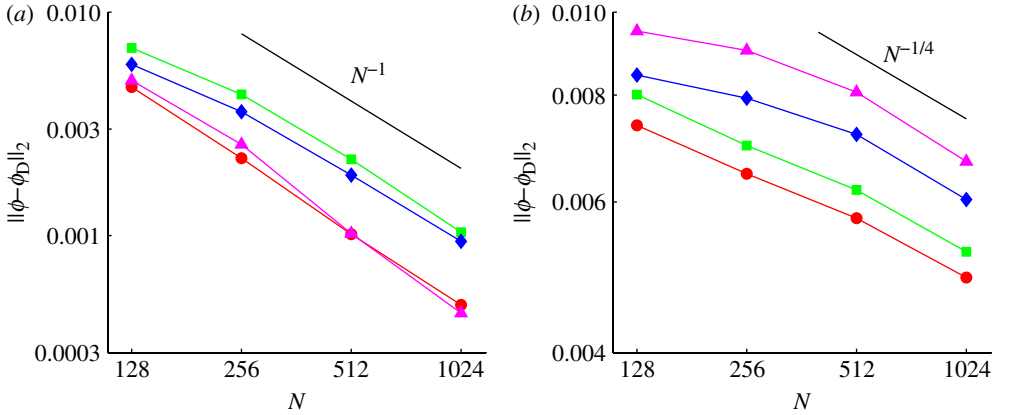

Figure 4. Convergence of the four components $\phi^{\pm}_{1,2}$ towards the reference solutions at (*a*) $t = 100$ and (*b*) $t = 400$ as the number of grid points N increases. Filled circles, ϕ^{+}_{1}; filled squares, ϕ^{+}_{2}; filled diamonds, ϕ^{-}_{1}; filled triangles, ϕ^{-}_{2}. (Online version in colour.)

initially related by $||\phi^{-}_{2}||^2 = 2||\phi^{-}_{1}||^2$, as expected for solutions in which ϕ^{+}_{1} is spherically symmetric and $||\phi^{+}_{2}|| \ll ||\phi^{+}_{1}||$. Again, the numerical solutions diverge away from this relation when $t \approx 100$. However, at $t = 100$, we still have the first-order convergence of all four components $\phi^{\pm}_{1,2}$ of the QLB solutions towards the reference solution, as shown in figure 4*a*. The rate of convergence deteriorates at later times, owing to the apparent sensitivity of the solution for $t \approx 100$. The measured convergence rate at $t = 400$ is only $N^{-1/4}$ over the range of resolutions used, as shown in figure 4*b*.

6. Conclusion

The QLB schemes are viable numerical schemes for solving the Dirac equation, not just for recovering its non-relativistic limit. Each step within the schemes is unitary, and at least second-order accurate. However, the overall schemes are only first-order accurate owing to operator splitting. We presented numerical evidence of first-order convergence towards highly accurate reference solutions for all four components of the Dirac wave function. The oscillations seen in the numerical output of QLB schemes that are not present in the Schrödinger equation are explained as relativistic effects owing to the finite mass of the particle.

We thank Silvia Palpacelli and Sauro Succi for useful conversations. P.J.D.'s research is supported by an EPSRC Advanced Research Fellowship, grant number EP/E054625/1. D.L. is supported by an attached project studentship. The computations made use of the FFTW3 library [16] and the Oxford Supercomputing Centre facilities.

References

1 Chen, S. & Doolen, G. D. 1998 Lattice Boltzmann method for fluid flows. *Annu. Rev. Fluid Mech.* **30**, 329–364. (doi:10.1146/annurev.fluid.30.1.329)

2 Succi, S. 2001 *The lattice Boltzmann equation: for fluid dynamics and beyond*. Oxford, UK: Oxford University Press.
3 Benzi, R., Succi, S. & Vergassola, M. 1992 The lattice Boltzmann equation: theory and applications. *Phys. Rep.* **222**, 145–197. (doi:10.1016/0370-1573(92)90090-M)
4 Succi, S. & Benzi, R. 1993 Lattice Boltzmann equation for quantum mechanics. *Physica D* **69**, 327–332. (doi:10.1016/0167-2789(93)90096-J)
5 Berestetskii, V. B., Lifshitz, E. & Pitaevskii, L. P. 1982 *Quantum electrodynamics*, 2nd edn. London, UK: Butterworth-Heinemann.
6 Succi, S. 1996 Numerical solution of the Schrödinger equation using discrete kinetic theory. *Phys. Rev. E* **53**, 1969–1975. (doi:10.1103/PhysRevE.53.1969)
7 Palpacelli, S. & Succi, S. 2007 Numerical validation of the quantum lattice Boltzmann scheme in two and three dimensions. *Phys. Rev. E* **75**, 066704. (10.1103/PhysRevE.75.066704)
8 Bialynicki-Birula, I. 1994 Weyl, Dirac, and Maxwell equations on a lattice as unitary cellular automata. *Phys. Rev. D* **49**, 6920–6927. (doi:10.1103/PhysRevD.49.6920)
9 Meyer, D. A. 1996 From quantum cellular automata to quantum lattice gases. *J. Statist. Phys.* **85**, 551–574. (doi:10.1007/BF02199356)
10 Palpacelli, S. & Succi, S. 2008 The quantum lattice Boltzmann equation: recent developments. *Commun. Comput. Phys.* **4**, 980–1007.
11 Whitham, G. B. 1974 *Linear and nonlinear waves*. New York, NY: Wiley Interscience.
12 He, X., Chen, S. & Doolen, G. D. 1998 A novel thermal model of the lattice Boltzmann method in incompressible limit. *J. Comput. Phys.* **146**, 282–300. (doi:10.1006/jcph.1998.6057)
13 Dellar, P. J., Lapitski, D., Palpacelli, S. & Succi, S. 2011 Isotropy of three-dimensional quantum lattice Boltzmann schemes. *Phys. Rev. E* **83**, 046706. (doi:10.1103/PhysRevE.83.046706)
14 Valdivieso, M. A. & Muñoz, J. D. 2009 Numerical comparison of 1D quantum lattice Boltzmann models. *J. Statist. Mech.* **2009**, P06004. (doi:10.1088/1742-5468/2009/06/P06004)
15 Forest, E. & Ruth, R. D. 1990 Fourth-order symplectic integration. *Physica D* **43**, 105–117. (doi:10.1016/0167-2789(90)90019-L)
16 Frigo, M. & Johnson, S. G. 2005 The design and implementation of FFTW3. *Proc. IEEE* **93**, 216–231. (doi:10.1109/JPROC.2004.840301)